Mechanical alloying and amorphization in Cu–Nb–Ag in situ composite wires studied by transmission electron microscopy and atom probe tomography

D. Raabe [a,*], S. Ohsaki [b], K. Hono [b]

[a] Max-Planck-Institut für Eisenforschung, Max-Planck-Str. 1, 40237 Düsseldorf, Germany
[b] National Institute for Materials Science, 1-2-1 Sengen, Tsukuba 305-0047, Japan

Abstract

We have studied deformation-driven alloying in a Cu–5 at.% Ag–3 at.% Nb in situ composite by transmission electron microscopy and atom probe tomography. In addition to alloying at interfaces, amorphization of nanosized Cu areas was observed after heavy wire drawing (true strain: $\eta = 10.5$) at some of the Cu–Nb interfaces. We discuss the alloying in terms of trans-phase dislocation-shuffling and shear banding mechanisms where lattice dislocations penetrate the interfaces between abutting phases. We interpret local amorphization in terms of the thermodynamic destabilization of a Cu–Nb crystalline phase between 35 and 80 at.% Cu due to enforced mixing. Deformation-driven mechanical alloying and amorphization are hence closely associated phenomena.
© 2009 Acta Materialia Inc. Published by Elsevier Ltd. All rights reserved.

1. Introduction

Binary and ternary metal matrix composites (MMCs) with Cu as matrix and a body-centered cubic (bcc) transition metal (e.g. Nb, Fe, and Cr) [1–14] and/or face-centered cubic (fcc) Ag [16–20] as additional phase(s) have attracted attention because of their high work hardening combined with excellent electrical conductivity. Basic interest in these alloys is mainly driven by the aim of understanding co-deformation among the phases and by high-strength electric wire applications [23–28].

Cu and most bcc metals have small mutual solubility, leading to two-phase microstructures. Upon straining, the phases form thin filaments, rendering these alloys in situ MMCs. The high interface density obtained after large reductions leads to enormous Hall–Petch-type hardening as was first reported for pearlitic wires [29] and later for Cu MMCs [30–32]. For instance, alloys consisting of Cu and 15 at.% Nb reveal an ultimate tensile strength (UTS) of up to 2.2 GPa ($\eta = 12$) [3–5].

Cu and Ag form a eutectic system with limited solubility. Alloys with more than 6 at.% Ag form a Cu-rich primary phase and a Cu–Ag eutectic. During deformation the eutectic and the Cu-rich matrix form into filaments with similar microstructure and properties as Cu-bcc MMCs. Intermediate annealing leads to Ag precipitates; these can increase the matrix strain and/or form additional fibers during deformation. After large strains, Cu–Ag MMCs reveal an UTS of up to $\sigma = 1.5$ GPa ($\eta = 10$) [17–19]. As in the case of Cu-bcc alloys, the increase in strength of Cu–Ag follows a Hall–Petch law. The strength and electrical conductivity of near-eutectic Cu–Ag alloys show a dependence on strain similar to that of Cu-bcc alloys. Due to the high conductivity of the constituents and the comparatively small contribution of inelastic electron scattering at interfaces, eutectic Cu–Ag MMCs reveal, at a

---

* Corresponding author. Tel.: +49 211 6792 278/340; fax: +49 211 6792 333.
E-mail address: d.raabe@mpie.de (D. Raabe).

given strength level, a somewhat better electrical conductivity than Cu-bcc alloys. Based on these binary systems, ternary Cu-bcc-Ag composites were developed to combine the hardening of all three phases and the interfaces between them and at the same time reduce the melting point [33–38].

Our current interest in these MMCs is fourfold. First, they are promising materials for magnet design [23–28] and robotics [36,37] owing to their excellent combination of strength and conductivity. Second, they are model composites for studying fundamental relations between strained lamellar microstructures on the one hand, and mechanical and electrical properties on the other. Third, heavily deformed MMCs can undergo strain-induced chemical mixing (mechanical alloying) far beyond equilibrium thermodynamics [10,11,39]. Fourth, they can even experience deformation-driven amorphization at the hetero-phase interfaces [6,11,40–42].

The first two aspects have been discussed in detail before [1–38]. The enormous strength of these compounds is attributed to a Hall–Petch effect [30–32] and the generation of geometrically necessary dislocations [2,4]. The resistive [1,6,7] and superconducting [34,43–46] properties in case of Nb-containing MMCs were discussed on the basis of the mean free path of conduction electrons (in Cu) and Cooper-pairs (in Nb), respectively, as a function of the interface spacing.

The latter two phenomena, however, are not well understood although they are of basic relevance for heavily deformed MMCs. In this work, therefore, we study possible mechanisms of deformation-driven chemical mixing among abutting phases (mechanical alloying) and the partial loss of crystalline structure of small interfacial Cu layers (deformation-driven amorphization) at high wire strains. We use a three-phase Cu–5 at.% Ag–3 at.% Nb alloy as model material for two reasons. First, the underlying binary systems, Cu–Nb [1–16] and Cu–Ag [17–20], have been studied in detail. Second, the material contains Cu–Ag, Cu–Nb and Nb–Ag phase boundaries so that three types of interface regions can be analyzed using the same specimen and boundary conditions. The properties of this materials and its microstructure were discussed in Refs. [33–35]. The wire has a UTS of 1840 MPa and 46% of the conductivity of pure Cu (IACS, International Annealed Copper Standard) at a wire strain of $\eta = 10.5$.

2. Processing and microstructure characterization

Processing of the Cu–5 at.% Ag–3 at.% Nb wires (max. true strain: $\eta = 10.5$) is described in Refs. [33–35,47]. Scanning and transmission electron microscopy (SEM, TEM) were used for microstructure characterization in longitudinal and cross-sections. Conventional TEM, high-resolution TEM and energy-filtered element maps (jump ratio method) were conducted using a Philips CM200 TEM, a JEOL 4000EX TEM, and a JEOL 2010F with a Gatan imaging filter, respectively. Longitudinal sections for TEM study were prepared by ion milling after grinding

and dimpling. A straight type atom probe with CAMECA's tomographic atom probe detection system (APT) was used to map the deformation-driven mixing among the phases (pulse fraction 0.15, pulse rate 600 Hz, specimen temperature 60 K, pressure $\sim 10^{-10}$ Torr). Field ion microscopy (FIM) specimens were prepared by electropolishing with 30% HNO_3 + 70% H_2O. FIM images were observed from the transverse direction at a temperature of 60 K at 9.2 kV using Ne as imaging gas.

3. Experimental results

3.1. Evolution of filament microstructure

Fig. 1 shows TEM bright- and dark-field images of the wires in longitudinal (a–c) and cross-sections (d–f) for $\eta = 7.5$, 8.6 and 10 ($\eta = \ln(A_0/A)$, where A is the wire cross-section). The fiber morphology in the longitudinal sections is rather uniform. For $\eta = 7.5$ the cross-section reveals the typical curling shape (Fig. 1d) which is due to the incompatibility between the cylindrical boundary conditions imposed by wire drawing and the plane strain response of the fibers. At $\eta = 7.5$ an average fiber thickness of 92.6 nm and at $\eta = 10$ of 53.7 nm was observed (cross-sections). The cross-sectional morphologies of the matrix at $\eta = 7.5$ and 10 are equiaxed and many of the grains are free from diffraction contrast, suggesting that they are recrystallized Cu (confirmed by separate dark-field and energy filtering images). The smallest Ag filaments ($\eta = 10$) were below 5 nm in thickness (Fig. 2). These observations are in accordance with earlier work [33–35].

3.2. Mechanical alloying

During wire drawing, the phases undergo deformation-induced mixing. This phenomenon is also known to occur for such MMCs during other high-strength deformation processes [48–51]. Fig. 3 shows energy-filtered images of wire cross-sections after $\eta = 7.5$ and $\eta = 10$. It was not possible to distinguish Ag and Nb by energy-filtered images, and hence only Cu and Ag maps obtained by the jump ratio method are shown. The filaments have curled shapes.

Fig. 4 shows nano-beam energy dispersive X-ray spectroscopy (EDS) data obtained on wire cross-sections ($\eta = 7.5$, $\eta = 10$). Point 1 at $\eta = 7.5$ is a reference measurement in the Cu matrix. Point 2 hits a Nb filament. Points 3–6 indicate both Nb and Ag with varying fractions, partly because of the convolution effect of the EDS analysis. Point 7 marks a Ag fiber. The results indicate that initially three phases can be distinguished, namely fcc-Cu, fcc-Ag and bcc-Nb. The nano-beam EDS results at $\eta = 10$ show for all points the dominance of Cu. Points 1 and 2 show a minor contribution of Nb. Points 3–6 reveal a considerable contribution of Ag. These data indicate a strong coexistence particularly of Cu and Ag within the same beam probe.

Fig. 5 shows the FIM image and the element maps at $\eta = 7.5$. Due to its higher evaporation field the Nb has a
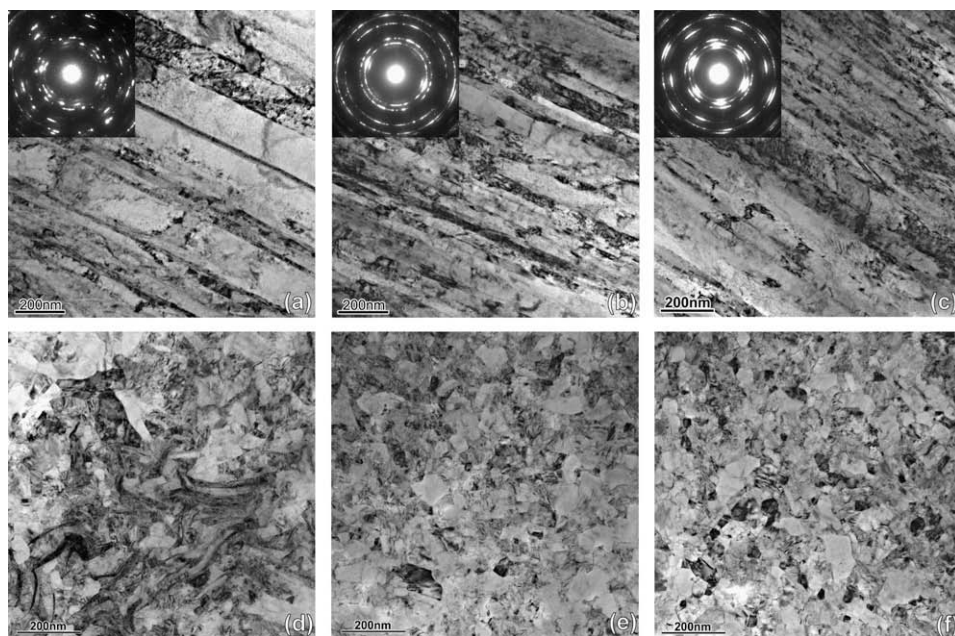
Fig. 1. Longitudinal sections (a–c) and cross-sections (d–f) of the wire-drawn material in TEM bright-field images for strains of $\eta = 7.5$, 8.6 and 10 ($\eta = \ln(A_0/A)$, where A is the wire cross-section).
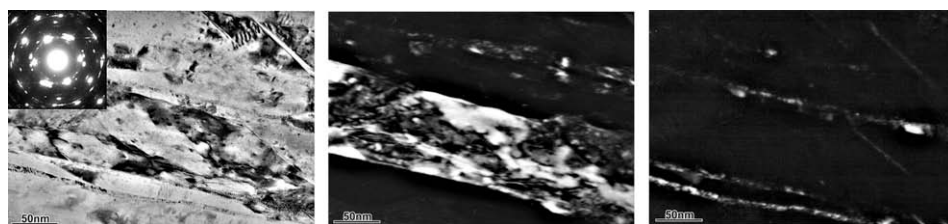

Fig. 2. TEM bright-field (a) and dark-field (b and c) images excited with Cu (1 1 0) (b) and Ag (2 0 0). The thickness of the Ag filaments is only ~5 nm.
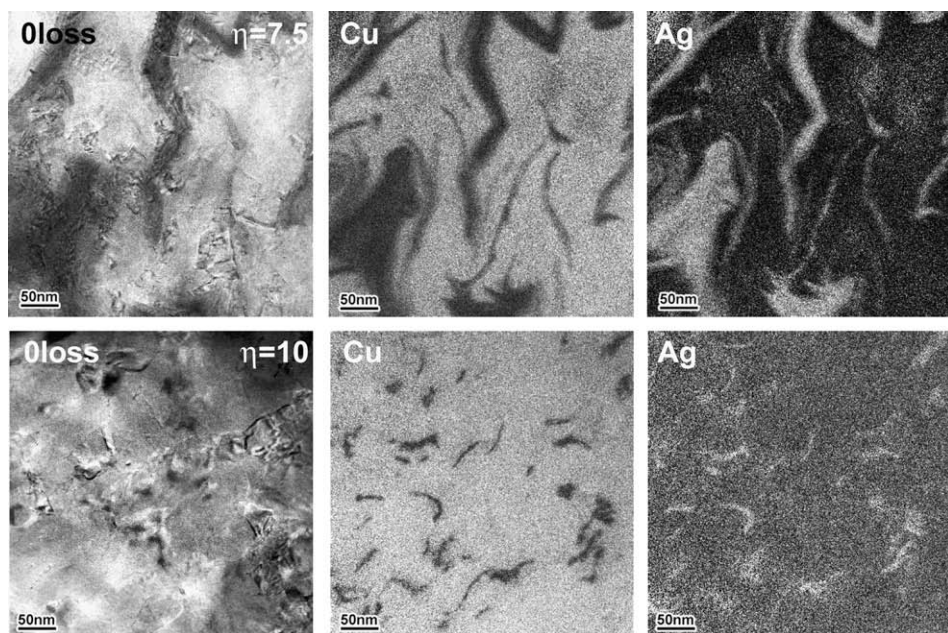

Fig. 3. Energy-filtered images of wire cross-sections after a strain of $\eta = 7.5$ and $\eta = 10$, respectively.
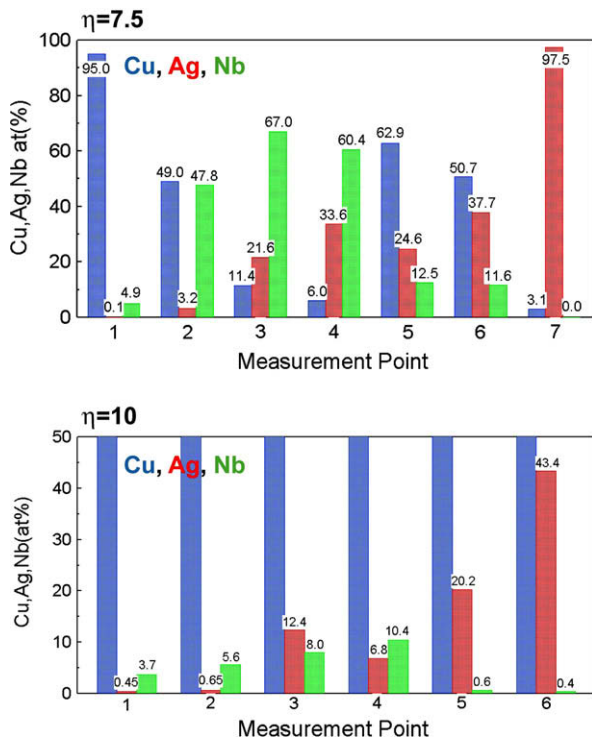
Fig. 4. Nano-beam EDS analysis on wire cross-sections at $\eta = 7.5$ and $\eta = 10$, respectively.

bright FIM contrast, while the Cu matrix appears dark. The atom probe data reveal a deformation-induced chemical

mixing in the Nb filament with a composition of 70–90 at.% Cu, 10–30 at.% Nb and about 5 at.% Ag. It should be noted that the Ag concentration is rather uniform throughout the two phases and the Nb concentration in the initial stage must have been nearly 100% in the Nb filament, as Nb has little solubility in Cu and Ag [33–35,47].

Fig. 6 shows a FIM image at $\eta = 10$ taken in the longitudinal direction of the wire. Nb and Ag filaments can both be observed in the dimly imaged Cu matrix. The Nb and Ag filaments can be distinguished because the Nb filament appears as a blurred bright image due to its high evaporation field. Initially, atoms were collected exclusively from the Nb filament. Since the Nb filament was very thin, the atoms were subsequently collected exclusively from the Cu matrix after the Nb filament was completely field evaporated. Therefore, this elemental map is not subject to the effect of local magnification, i.e. the concentration profile in Fig. 6c is considered to be rather reliable. The APT map of Nb and Cu shows a Nb filament contacting the Cu matrix with a curved interface. The composition profile shows nearly complete mechanical mixing of the two (non-soluble) elements in the Nb filament. The mechanically alloyed Nb contains about 50 at.% Cu, 40 at.% Nb and 6 at.% Ag. In the transition zone between the Nb and the Cu matrix (3.5–6 nm) we observe a content of ~10 at.% Ag. The interface area reveals a Cu gradient which is wider than observed at the Nb filament after $\eta = 7.5$ (Fig. 5).

Fig. 7 shows an APT map of a Ag filament observed at $\eta = 10$ and the corresponding concentration–depth profile
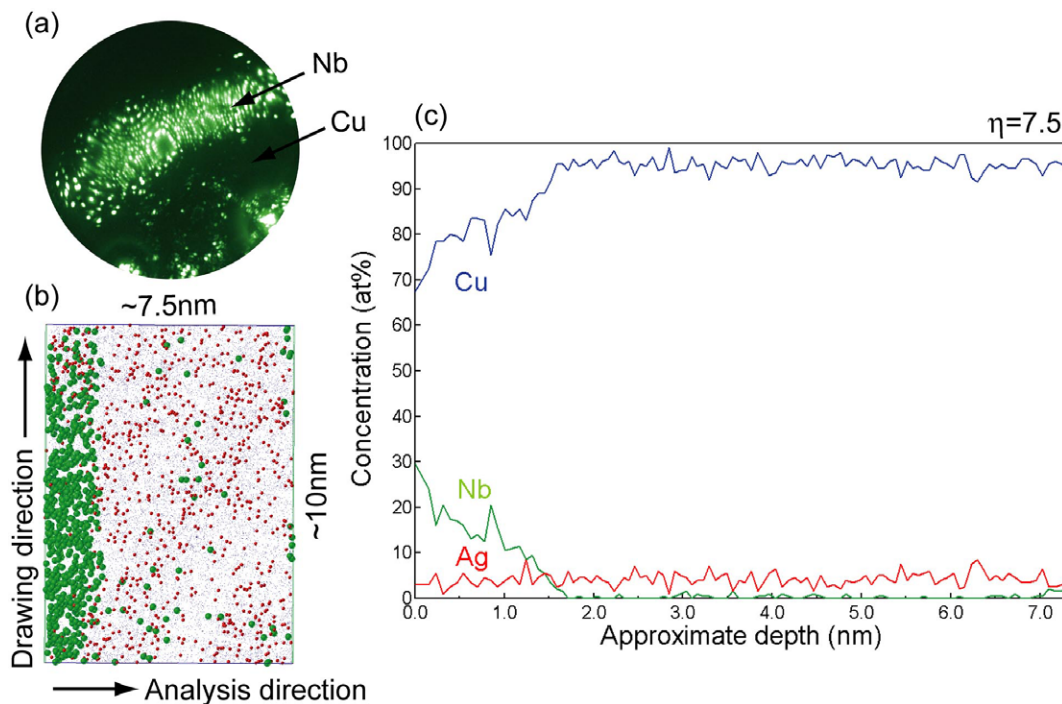

Fig. 5. Deformation-induced chemical mixing ($\eta = 7.5$) at the interface between the Cu matrix and a Nb filament. The FIM image (a) shows the bright-appearing Nb (higher evaporation field than Cu). The composition profile (c) is obtained by atom probe tomography (b). The mechanically alloyed region contains 70–90 at.% Cu, 10–30 at.% Nb, and about 10 at.% Ag. Color code: Cu, blue; Nb, green; Ag, red.
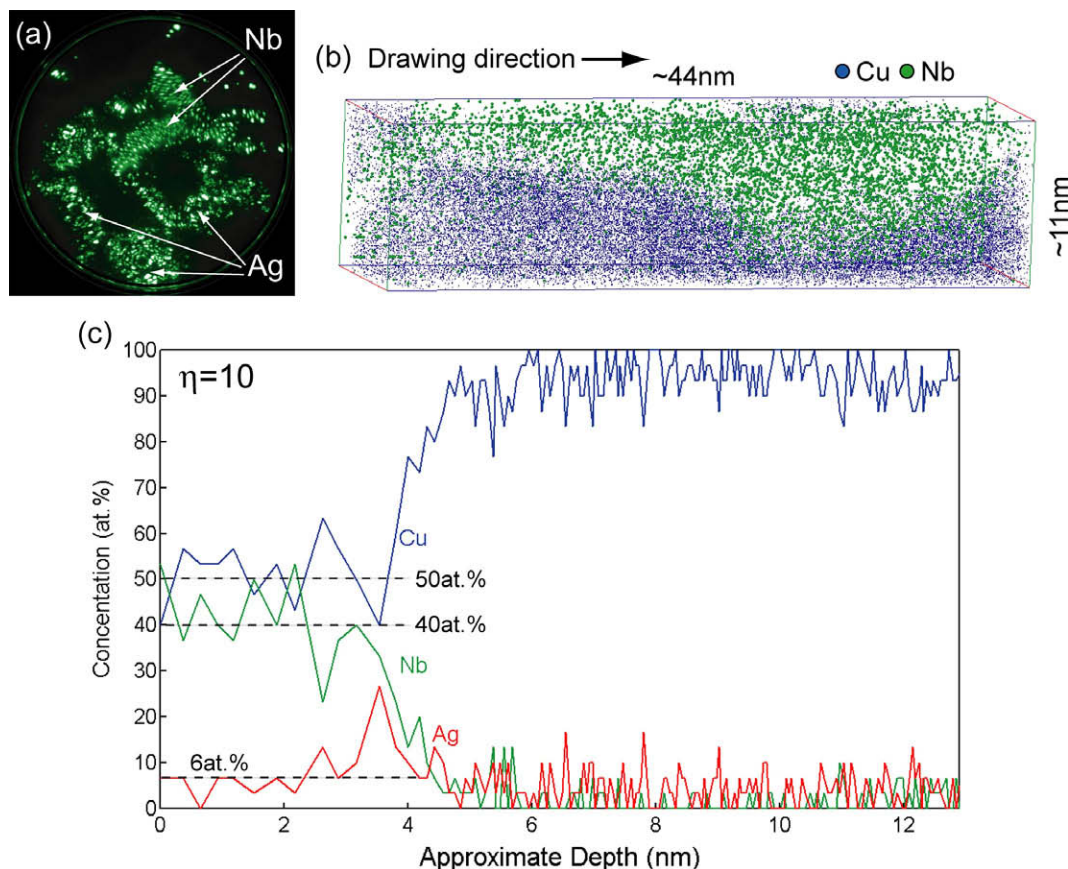
Fig. 6. Deformation-induced chemical mixing ($\eta = 10$) at the interface between the Cu matrix and a Nb filament. The profile is obtained by atom probe tomography. The mechanically alloyed region contains about 50 at.% Cu, 40 at.% Nb and 10 at.% Ag. Color code: Cu, blue; Nb, green; Ag, red.

calculated from the inset region. The mechanical alloying effect is even stronger in the Ag fibers. The ladder diagram taken in cross-section (Fig. 7a) shows that the Ag-rich zone, where the original fiber is located, has a Ag content of only 14.5 at.%. Outside of this zone the Ag content drops to a value of 3.2 or 4 at.%.

3.3. Deformation-driven amorphization

Fig. 8a shows a high dislocation density ($\perp$ symbols) within a Ag filament (about $4 \times 10^{16} \, \text{m}^{-2}$) surrounded by Cu ($\eta = 10$). Amorphous layers are not observed. Fig. 8b shows a high dislocation density also in the Nb and an amorphous zone in the Cu at the Nb/Cu interface ($\eta = 10$). Amorphous layers were observed only at Nb/Cu interfaces. The adjacent Nb crystal structure seems to be intact. The width of the area where amorphization occurs agrees with the range of the mechanical mixing zone observed by APT.

4. Discussion

We observe deformation-driven chemical mixing (mechanical alloying) between Cu–Nb and Cu–Ag (Figs. 3–7), i.e. the compositions at these interfaces after heavy wire drawing lie far above the equilibrium limits.

Mechanical alloying has been studied in a number of related Cu-based alloys (e.g. Cu–Nb [39–42], Cu–Fe [49–56], Cu–Ag [18,19,33–37,61–63], Cu–V [64], Cu–Co [65], Cu–Cr [14,36,37,66] and Cu–Zr [67]) deformed by heavy straining (e.g. milling, drawing, rolling, torsion). An overview on these systems regarding forced alloying and thermodynamics is given in Ref. [68]. Figs. 6–8 show that in the present case mechanical alloying leads not only to mixing of the abutting phases but even to the gradual dissolution of the minority phase (Fig. 7). Regarding the latter case (Fig. 7), an alternative to the hypothesis of a dissolving Ag fiber might be that the Ag-rich domain is a segregation zone on a Cu grain boundary.

Three groups of approaches are conceivable for explaining chemical mixing during co-deformation of phases consisting of non-soluble elements. The first one assumes a purely diffusion-driven mechanism [69]. The second one assumes defect-enhanced diffusion (dislocations, vacancies) [53,58,68,69]. The third one is mainly based on mechanical mixing (and subsequent short-range diffusion) via shear transfer (dislocations, shear bands) across hetero-phase interfaces (referred to as shuffling) [70,71]. Besides discussing the lattice defect kinetics associated with such mechanisms, we also address thermodynamic aspects of the problem (equilibrium [68], non-equilibrium (driven systems) [72,73] and defactant effects [74,75]). Finally, the
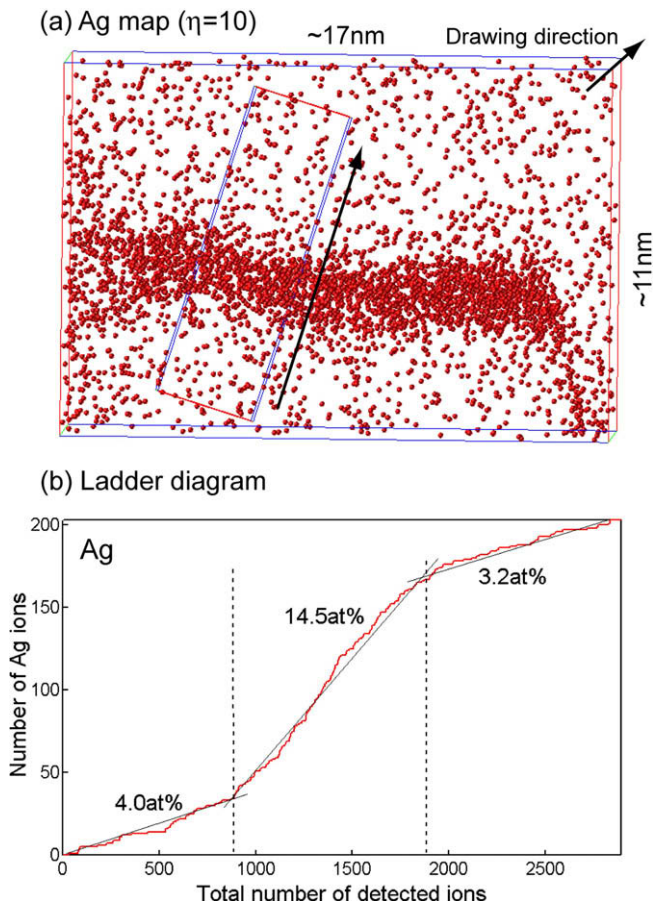
Fig. 7. (a) Deformation-induced chemical mixing ($\eta = 10$) between Cu matrix and Ag filaments. Atom probe tomography data in cross-sections and as ladder diagram (Ag). The mechanically alloyed Cu–Ag region contains about 70–82 at.% Cu and 18–30 at.% Ag. Color code: Cu, blue; Ag, red.

Fig. 8. (a) Dislocations within a Ag filament ($\perp$ symbols) at a wire strain of $\eta = 10$. The dislocation density inside the filament is $4 \times 10^{16}\,\mathrm{m}^{-2}$. The surrounding material is the Cu matrix. (b) High dislocation density in the Nb filament (Nb) and amorphization (Amo) of the Cu matrix (Cu) at a wire strain of $\eta = 10$.

amorphization phenomenon is discussed in the context of the enforced mixing.

4.1. Diffusion mechanism

A purely diffusion-driven approach can be ruled out for explaining forced chemical mixing in the present case as Cu–Nb and Cu–Ag have negligible equilibrium solubility. In the Cu–Nb phase diagram the maximum solubility is about 0.1 at.% Nb in Cu and 0.6 at.% Cu in Nb between 800 and 1000 °C. For Cu–Ag the maximum solubility is 5–6 at.% Ag in Cu at 780 °C. The maximum solubility of Cu in Ag at about 780 °C is 14 at.%. Solubilities drop below 0.1 at.% at room temperature. This means that the massive alloying shown in Fig. 6 for Cu–Nb (about 50 at.% Cu, 40 at.% Nb, 10 at.% Ag) and Fig. 7 for Cu–Ag (about 70–82 at.% Cu, 18–30 at.% Ag) are not created by regular diffusion owing to the absence of thermodynamic driving forces, i.e. the observed compositions are not characterized by a negative enthalpy of mixing. Considering further thermodynamic contributions such as capillary pressure (Gibbs–Thomson effect) and internal stresses does
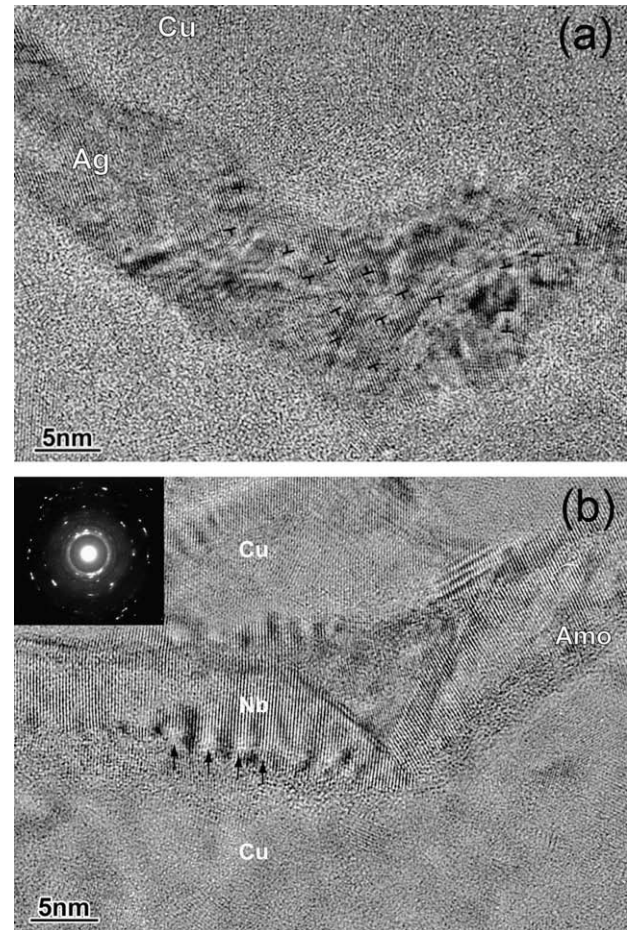
also not provide a negative mixing enthalpy for the present case [68,72,73].

The absence of a sufficient driving force for spontaneous interdiffusion and phase dissolution is also evident from annealing experiments which show that wire-drawn and mechanically alloyed MMCs undergo immediate demixing and gradual spherodization rather than further diffusion-driven alloying [38,76–77].

4.2. Defect-assisted diffusion

The second group of approaches for explaining mechanical mixing is based on plasticity-assisted (short-range) diffusion. The respective mechanisms and their contributions to mixing are discussed with different emphasis in the literature. Farber [78] and Khina and Formanek [79] explain accelerated diffusion in binary systems through a deformation-induced increase in the non-equilibrium vacancy density [69]. They assume that these additional diffusion carriers lead to chemical mixing across the interface. Although this effect is in principle possible, two arguments

stand against it for explaining our observations. First, all phases in the alloy, i.e. Cu, Ag and Nb, are plastically strained, though not to the same extent [33–35]. This means that an increased vacancy concentration should be present in all phases. Second, if higher defect densities enhance diffusion, the resulting mixing profiles should be symmetric, which is not the case. Hence, we concede that increased diffusion is indeed likely within the phases and possibly also across the hetero-phase interfaces but not necessarily with a net flux in either direction, i.e. this effect cannot explain the massive non-symmetric interphase mixing observed in the current material.

Instead, it is more plausible to assume a two-step mixing mechanism consisting of an athermal, plastic part and a thermal, diffusional part. In the first step lattice dislocations arrive in the interfaces pushing rows of atoms via shear into the neighboring phase and misfit dislocations into the interface. This effect leads to atomic-scale interface roughening. Different suggestions were made regarding the next step of this process [53–60,68,69]. One group of models suggests that a certain number of atoms located at the interface steps spontaneously cross the interface and diffuse into the opposite phase. As an additional effect it was discussed that diffusion might be accelerated as the kinetic energy of atoms increases due to the mechanical forces of the incoming dislocation flux (ballistic effects). In addition, the argument of a deformation-induced increase in the vacancy density as discussed above has been addressed in this context.

Again, this approach is not entirely plausible as the thermodynamic driving forces created by such a dislocation flux (and an increased vacancy density) are still not high enough to justify massive interdiffusion (see Fig. 8a). Eckert et al. [53,58] and Schwarz [69] suggested a related mechanism based on dislocation shear plus subsequent pipe diffusion. These authors assumed segregation and subsequent diffusion of solutes to the dislocation cores in the neighboring phase. Pipe diffusion is fast enough for solute penetration into the other phase. Further, it was suggested that upon dislocation motion and depinning, solutes are left behind, leading to a supersaturated solid solution. While the pipe-diffusion mechanism seems kinetically more realistic, the same counter-argument as above applies. This means that the fact that pipe diffusion is much faster than regular lattice diffusion does not resolve the dilemma of an insufficient driving force for massive net diffusion of atoms from one phase into the other. A faster diffusion mechanism still does not explain why long-range chemical mixing takes place when the mixing enthalpy is positive. Also, as the phases in the current case co-deform and accommodate similar strains [33–35], sufficient dislocation densities are available in all phases, and hence the diffusion profiles should be symmetric, which is not the case.

An alternative possibility for the preferred thermodynamic stabilization of lattice dislocations on either side of an interface, serving as pipe carriers, might arise from the defactant theory of Kirchheim [74,75]. While this approach might provide a thermodynamically more plausible account of this phenomenon, a contradiction remains as short-term annealing of wire-drawn MMCs generally leads to demixing rather than to further mixing [38,76–77].

Some kinetic and thermodynamic aspects of these mechanisms were discussed by Ma et al. [68] and Martin [72,73]. These authors come to similar conclusions, namely that irrespective of kinetic support provided by pipe diffusion or additional vacancies, the thermodynamic driving forces are not large enough for spontaneous intense alloying in a system with very small mutual solubility.

4.3. Dislocation-shuffling and shear banding

Various authors have discussed the possibility of dislocation glide across hetero-interfaces [8,70,71,80–89]. It may be assumed that slip transmission among abutting phases can be considered in analogy to single-phase slip transfer across high-angle grain boundaries [80–82]. Embury and co-workers [83] suggested criteria that promote hetero-phase slip transfer. First, the resolved shear stress of the dislocations approaching the interface should be a maximum on the activated system. Second, the misorientation between the active slip planes on either side of the interface should be a minimum at the boundary. Third, the configuration at the interface should be one of minimum energy.

Concerning the current Cu–Ag–Nb alloy [33–35] such conditions are fulfilled for the co-deformation of the two fcc phases Cu and Ag. Both materials form a $\langle 1\,1\,1 \rangle$ texture in the wire [6,32–35], i.e. the orientations of the highly stressed slip systems match. The bcc-Nb forms a $\langle 1\,1\,0 \rangle$ texture [6,32,43–46] which leads to Kurdjumov–Sachs coincidence of the leading slip systems. The orientation factor for the most highly stressed slip system in Cu and Ag with $\langle 1\,1\,1 \rangle$ texture is 0.27 and for Nb with $\langle 1\,1\,0 \rangle$ texture 0.4. The misorientation between the active slip systems in the Cu matrix phase and the two minority phases, Ag and Nb, is nearly zero. In that case the Burgers vectors of the misfit dislocations that are created in the interfaces are relatively small ($b_{Cu} = 0.255$ nm, $b_{Nb} = 0.286$ nm, $b_{Ag} = 0.288$ nm). The high dislocation content we observed in the Nb filament directly adjacent to the amorphous Cu–Nb region supports this hypothesis as an explanation for mechanical alloying in the present case (arrows in Fig. 8b).

It is likely, however, that dislocation-shuffling across hetero-phase interfaces becomes active only at high flow stresses and nanoscale fiber diameters. Fibers with a micrometer-scale diameter can be deformed like a regular grain, i.e. through in-grain dislocation multiplication and glide. The transition from conventional in-grain dislocation plasticity to trans-phase slip transfer is suggested to occur in three steps during heavy deformation. In the case of bulk two-phase plasticity, classical Hall–Petch interface mechanics applies (phase I). When the filaments become thinner, dislocation half-sources or interface sources become active and plasticity is dominated by Orowan

expansion within the lamellae (phase II) [84–86]. If the filaments reach the nanometer scale, slip transmission takes place (phase III) [85–90].

Regarding this situation, it is likely that at low strains the interface acts as a conventional barrier to dislocation motion in the softer matrix phase (Cu in our case) and as a source of dislocations in the embedded phase (Nb, Ag in the present case) [87]. At higher strains and smaller fiber dimensions slip transmission across the interface is suggested to create residual interface dislocations that may rearrange by glide or climb [87]. Wang et al. [89,90] published atomistic and elasticity predictions which suggest that inbound lattice dislocations may even preferably enter the interface rather than penetrating it. Embury et al. [83,87,89,88] discussed that in heavily deformed materials the dimensions of the filaments may be so small that dislocation–dislocation interactions within the constituent phases may be less important and that, instead, dislocation production and storage occurs predominantly at the interfaces. This is analogous to phase III discussed above: deformation is then determined by shear transfer across the interfaces, leading to mechanically induced chemical mixing, and additional energy storage through the production of additional interfacial area with plastic strain (Fig. 9).

Besides dislocation-shuffling, shear banding could be a supporting mechanism to explain cross-interface deformation and chemical mixing. Ohsaki et al. [67] and Embury and co-workers [83] discussed shear banding as a deformation mode during two-phase co-deformation at the respective interfaces. Examples exist for Cu–Zr, Cu–Nb, α–β brass, Cu–Cr, Ni–W and Cu–Ag.

Based on these considerations we assume that transphase plastic deformation (dislocation shuffling, probably assisted by shear banding) can explain the observed forced alloying. This means that shearing of atomic planes through dislocation glide on more than one slip system across the interface of very thin abutting layers can create small embedded particles consisting of atoms from one phase in the other. Such tiny material portions can be further cut by dislocations running through them, thereby increasing their energy through the Gibbs–Thomson effect so that they finally dissolve [68,70,71,91,92] (Fig. 9).

4.4. Deformation-driven amorphization

Before discussing possible explanations for the solid-state amorphization observed in this work, we briefly summarize some key features of the phenomenon including observations from earlier studies on wire drawing. The effect seems to occur particularly in composites with high negative enthalpy of mixing [6,11,40–42,67,93]. Pure Cu, Ag and Nb wires do not become amorphous during wire drawing. This observation indicates that a relationship exists between mechanical alloying, the enthalpy of mixing of the newly formed compounds, and subsequent amorphization. This argument is supported by the fact that the abutting phase of an amorphous Cu region frequently shows high dislocation densities (Fig. 8b). The relationship between mechanical mixing and amorphization seems to apply in particular to the Cu matrix, which becomes amorphous only when mechanically alloyed. Deformation-induced amorphization of Cu during wire drawing was reported in Cu–Nb, Cu–Nb–Ag (Fig. 8b) and Cu–Zr (Fig. 10) [6,11,40–42,67]. In all cases at least one pair of the constituent elements reveal a negative enthalpy of mixing.

According to the Gibbs free energy–concentration diagram calculated by ThermoCalc (Fig. 11), an amorphous Cu–Nb phase could indeed be stable at 25 °C for Cu
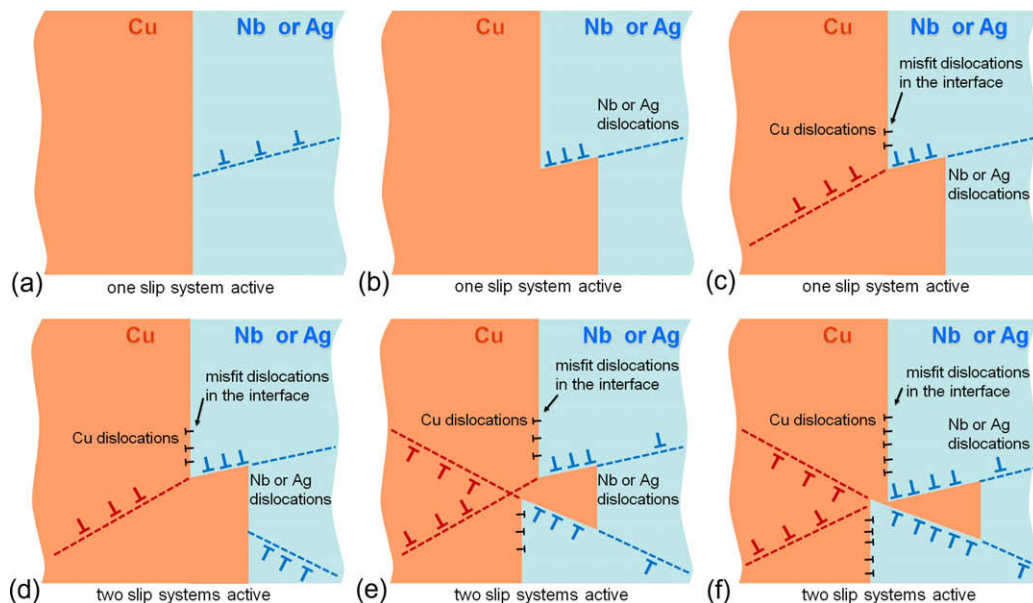

Fig. 9. Schematic image which shows how the first step of mechanical alloying can be explained by a dislocation shuffle mechanism.
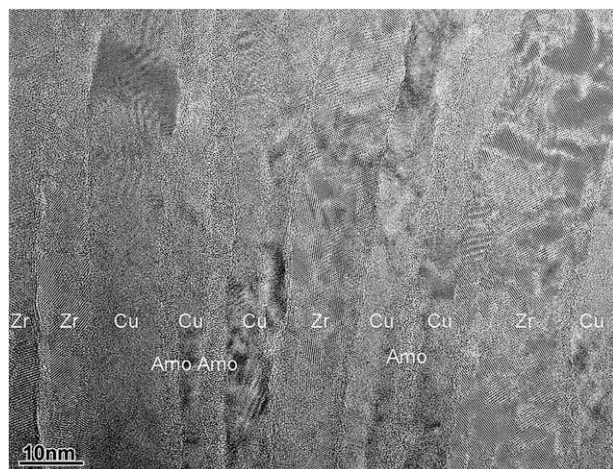
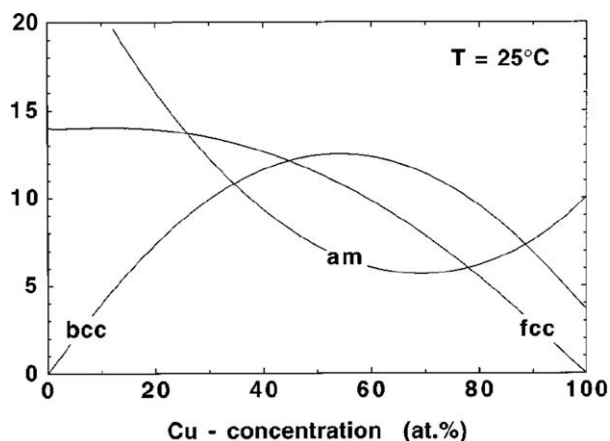Fig. 10. Amorphization of accumulative roll-bonded Cu/Zr multilayer. Adapted with permission from Ref. [65].

Fig. 11. Free energy diagram of the Cu–Nb system calculated by ThermoCalc. "am" refers to the amorphous phase which is stable for alloys between 35 and 80 at.% Cu.

concentrations between 35 and 80 at.% relative to the bcc and fcc solid solutions that could be formed by forced mixing. Our current measurements (Fig. 6) fall in this regime. The atomic radius mismatch is 12.1% for Cu–Nb, 13.1% for Cu–Ag and even 24.4% for Cu–Zr.

Another approach to explain amorphization in the current system would be to consider the change in the total free energy due to the dislocation energy [6]. This means that if the stored deformation energy increases upon straining, it is conceivable that a transformation into the amorphous regime is energetically favorable. This approach, however, does also not provide a sufficiently consistent explanation for the current case as we observed that many dislocations were absorbed at the Cu–Nb interfaces rather than being stored within the phases. This effect is also suggested by recent atomistic simulations of Wang et al. [89,90]. Furthermore, in the pure constituents (Cu, Ag, Nb), and in other MMCs which have been equally or even

more heavily deformed, stored dislocations alone were not found to be sufficient for spontaneous amorphization.

Owing to these considerations, it seems likely that amorphization has taken place in the current case via a two-step mechanism that consists, first, of a dislocation-shuffling or shear-band-related trans-phase plastic deformation and mixing process (Fig. 9); and second, of a gradual amorphization in regions where both heavy mixing and high dislocation densities exist. The transition seems to be particularly likely in systems which fulfill at least some of the classical glass-forming rules.

5. Conclusions

A ternary Cu–5 at.% Ag–3 at.% Nb in situ composite wire (max true strain $\eta = 10.5$) was studied using high-resolution HRTEM and atom probe tomography. Two main observations were made: (i) intense mechanical alloying occurred among all three phases (Cu, Nb, Ag); (ii) amorphization of small areas of Cu took place at some of the Cu–Nb interfaces. We explain the mechanical alloying process in terms of trans-phase dislocation-shuffling or shear band mechanisms where lattice dislocations penetrate the interfaces between abutting phases, leading to chemical mixing. We interpret the local amorphization of Cu at some of the Cu–Nb interfaces in terms of the thermodynamic stabilization of an amorphous Cu–Nb phase between 35 and 80 at.% Cu due to the preceding enforced mechanical mixing. Mechanical alloying and amorphization are hence associated phenomena in this system. We claim that this two-step mechanism can also be used to explain mechanical alloying and (at least partial) amorphization in other heavily deformed systems such as produced by roll bonding, milling, wire drawing or high-pressure torsion.

Acknowledgments

References

[1] Bevk J, Harbison JP, Bell JL. J Appl Phys 1978;49:6031.
[2] Funkenbusch PD, Courtney TH. Acta Metall 1985;33:913.
[3] Spitzig WA, Pelton AR, Laabs FC. Acta Metall 1987;35:2427.
[4] Funkenbusch PD, Lee JK, Courtney TH. Metall Trans A 1987;18:1249.
[5] Spitzig WA, Downing HL, Laabs FC, Gibson ED, Verhoeven JD. Metall Trans A 1993;24:7.
[6] Raabe D, Heringhaus F, Hangen U, Gottstein G. Z Metallk 1995;86:405.
[7] Heringhaus F, Raabe D, Gottstein G. Acta Metall 1995;43:1467.
[8] Wood JT, Embury JD, Ashby M. Acta Mater 1997;45:1099.
[9] Embury JD, Han K. Curr Opin Solid State Mater Sci 1998;3:304.

[10] Sauvage X, Thilly L, Lecouturier F, Guillet A, Blavette D. Nanostruct Mater 1999;11:1031.
[11] Sauvage X, Renaud L, Deconihout B, Blavette D, Ping DH, Hono K. Acta Mater 2001;49:389.
[12] Thilly L, Lecouturier F, Von Stebut J. Acta Mater 2002;50:5049.
[13] Hong SI, Hill MA. Scripta Mater 2001;44:2509.
[14] Lee KL, Whitehouse AF, Withers PJ, Daymond MR. Mater Sci Eng A 2003;348:208.
[15] Sandim MJR, Stamopoulos D, Sandim HRZ, Ghivelder L, Thilly L, Vidal V, et al. Supercond Sci Technol 2006;19:1233.
[16] Cline HE, Lee D. Acta Metall 1970;18:315.
[17] Frommeyer G, Wasseermann G. Acta Metall 1975;23:1353.
[18] Sakai Y, Inoue K, Maeda H. Acta Metall 1995;43:1517.
[19] Sakai, Schneider-Muntau HJ. Acta Metall 1997;45:1017.
[20] Heringhaus F, Schneider-Muntau HJ, Gottstein G. Mater Sci Eng 2003;347:9.
[21] Foner S, Bobrov E. IEEE Magn 1987;24:1059.
[22] Asano T, Sakai Y, Inoue K, Oshikiri M, Maeda H. IEEE Magn 1992;28:888.
[23] Heringhaus F, Eyssa YM, Pernambuco-Wise P, Bird MD, Gottstein G, Schneider-Muntau HJ. Metall 1996;50:272.
[24] Spencer K, Lecouturier F, Thilly L, Embury JD. Adv Eng Mater 2004;6:290.
[25] Embury JD, Hill MA, Spitzig WA, Sakai Y. MRS Bull 1993;8:57.
[26] Heringhaus F, Leffers R, Gottstein G, Schneider-Muntau HJ. Processing, properties, and application of cast metal matrix composites. TMS fall meeting, vol. 1; 1996. p. 127.
[27] Schneider-Muntau HJ. IEEE Trans Magn 1982;18:32.
[28] Botcharova E, Freudenberger J, Gaganov A, Khlopkov K, Schultz L. Mater Sci Eng A 2006;416:261.
[29] Langford G. Metall Trans 1970;1:465.
[30] Trybus C, Spitzig WA. Acta metall 1989;37:1971.
[31] Sevillano JG. J Phys III 1990;6:967.
[32] Hangen U, Raabe D. Acta Metall 1995;43:4075.
[33] Raabe D, Mattissen D. Acta Mater 1998;46:5973.
[34] Raabe D, Mattissen D. Acta Mater 1999;47:769.
[35] Mattissen D, Raabe D, Heringhaus F. Acta Mater 1999;47:1627.
[36] Miyake K, Hanzawa N, Takahara H, Kobayashi S, Raabe D. Jpn J Appl Phys 2000;39:119.
[37] Raabe D, Miyake K, Takahara H. Mater Sci Eng A 2000;291:186.
[38] Raabe D, Ge J. Scripta Mater 2004;51:915.
[39] Gong HR, Liu BX. J Appl Phys 2004;96:3020.
[40] Raabe D, Hangen U. Mater Lett 1995;22:155.
[41] Raabe D, Hangen U. J Mater Res 1995;10:3050.
[42] Wang TL, Li JH, Tai KP, Liu BX. Scripta Mater 2007;57:157.
[43] Raabe D, Heringhaus F. Phys Status Solidi A 1994;142:473.
[44] Hangen U, Raabe D. Phys Status Solidi (a) 1995;147:515.
[45] Raabe D, Hangen U. Acta Metall 1996;44:953.
[46] Raabe D, Hangen U. Phys Status Solidi (a) 1996;154:715.
[47] Mattissen D, Raabe D. Metall 1997;51:464.
[48] Wille C, Al-Kassab T, Schmidt M, Choi PP, Kwon YS. Int J Mater Res 2008;99:541.
[49] Jiang JZ, Gente C, Bormann R. Mater Sci Eng A 1998;242:268.
[50] Sauvage X, Wetscher F, Pareige P. Acta Mater 2005;53:2127.
[51] Wille C, Al-Kassab T, Choi PP, Kwon YS. Ultramicroscopy 2009;109:599.
[52] Huang JY, Yu YD, Wu YK, Li DX, Ye HQ. Acta Mater 1997;45:113.
[53] Eckert J, Holzer JC, Krill III CE, Johnson WL. J Appl Phys 1993;73:131 [and 2794].
[54] Schilling PJ, Palshin V, Tittsworth RC, He JH, Ma E. Phys Rev B 2003;68:224204.
[55] Jiang JZ, Gonser U, Gente C, Bormann R. Appl Phys Lett 1993;63:1056.
[56] Bellon P, Averback RS. Phys Rev Lett 1995;74:1819.
[57] Drbohlav O, Yavari AR. Acta Metall Mater 1995;43:1799.
[58] Eckert J, Holzer JC, Krill III CE, Johnson WL. J Mater Res 1992;7:1980.
[59] Fultz B, Ahn CC, Spooner S, Hong LB, Eckert J, Johnson WL. Metall Mater Trans A 1996;27:2934.
[60] Schilling PJ, He JH, Cheng J, Ma E. Appl Phys Lett 1996;68:767.
[61] Uenish K, Kobayashi K, Ishihara K, Shingu PH. Mater Sci Eng A 1991;134:1342.
[62] Najafabady R, Srolovitz DJ, Ma E, Atzmon M. J Appl Phys 1993;74:3144.
[63] Sheng HW, Wilde G, Ma E. Acta Mater 2002;50:475.
[64] Sakurai K, Mori M, Mizutani U. Phys Rev B 1992;46:5711.
[65] Gente C, Oehring M, Bormann R. Phys Rev B 1993;48:13244.
[66] Ogino Y, Yamasaki T, Murayama S, Sakai R. J Non-Cryst Solids 1990;117/118:737.
[67] Ohsaki S, Kato S, Tsuji N, Ohkubo T, Hono K. Acta Mater 2007;55:2885.
[68] Ma E, Sheng HW, He JH, Schilling PJ. Mater Sci Eng A 2000;286:48.
[69] Schwarz RB. Mater Sci Forum 1998;269–272:665.
[70] Gleiter H. Acta Metall 1968;16:455.
[71] Differt K, Essmann U, Mughrabi H. Phys Status Solidi (a) 1987;104:95.
[72] Pochet P, Tominez E, Chaffron L, Martin G. Phys Rev B 1995;52:4006.
[73] Martin G. Phys Rev B 1984;30:1424.
[74] Kirchheim R. Acta Mater 2007;55:5129 [and 5138].
[75] Kirchheim R. Int J Mater Res 2009;100:4.
[76] Ohsaki S, Yamazaki K, Hono K. Scripta Mater 2003;48:1569.
[77] Sandim HRZ, Sandim MJR, Bernardi HH, Lins JFC, Raabe D. Scripta Mater 2004;51:1099.
[78] Farber VM. Met Sci Heat Treat 2002;44:317.
[79] Khina BB, Formanek B. Defect Diffus Forum 2006;246:105.
[80] Kumar D, Bieler TR, Eisenlohr P, Mason DE, Crimp MA, Roters F, et al. J Eng Mater Technol (Trans ASME) 2008;130:021012-1.
[81] Bieler TR, Eisenlohr P, Roters F, Kumar D, Mason DE, Crimp MA, et al. Int J Plast 2009;25:1655.
[82] Roters F, Eisenlohr P, Hantcherli L, Tjahjanto D, Ma D, Bieler TR, et al. Acta Mater; submitted for publication.
[83] Sinclair CW, Embury JD, Weatherly GC. Mater Sci Eng A 1999;272:90.
[84] Gil Sevillano J. J Phys III 1991;1:967.
[85] Misra A, Hirth JP, Hoagland RG. Acta Mater 2005;53:4817.
[86] Embury JD, Hirth JP. Acta Method 1994;42:2051.
[87] Embury JD, Sinclair CW. Mater Sci Eng A 2001;319–321:37.
[88] Embury JD. Scripta Metall Mater 1992;27:981.
[89] Wang J, Hoagland RG, Hirth JP, Misra A. Acta Mater 2008;56:5685.
[90] Wang J, Hoagland RG, Hirth JP, Misra A. Acta Mater 2008;56:3109.
[91] Yavari AR. Mater Sci Eng A 1994;179/180:20.
[92] Drobohlav O, Yavari AR. Acta Mater 1995;43:1799.
[93] Borchers C, Al-Kassab T, Goto S, Kirchheim R. Mater Sci Eng A 2009;502:131.